The Innovation

Article

Restored relationship between ENSO and Indian summer monsoon rainfall around 1999/2000

Xianke Yang[1,2] **and Ping Huang**[1,3,*]

*Correspondence: huangping@mail.iap.ac.cn

Received: November 15, 2020; Accepted: March 30, 2021; Published Online: April 2, 2021; https://doi.org/10.1016/j.xinn.2021.100102

Graphical abstract

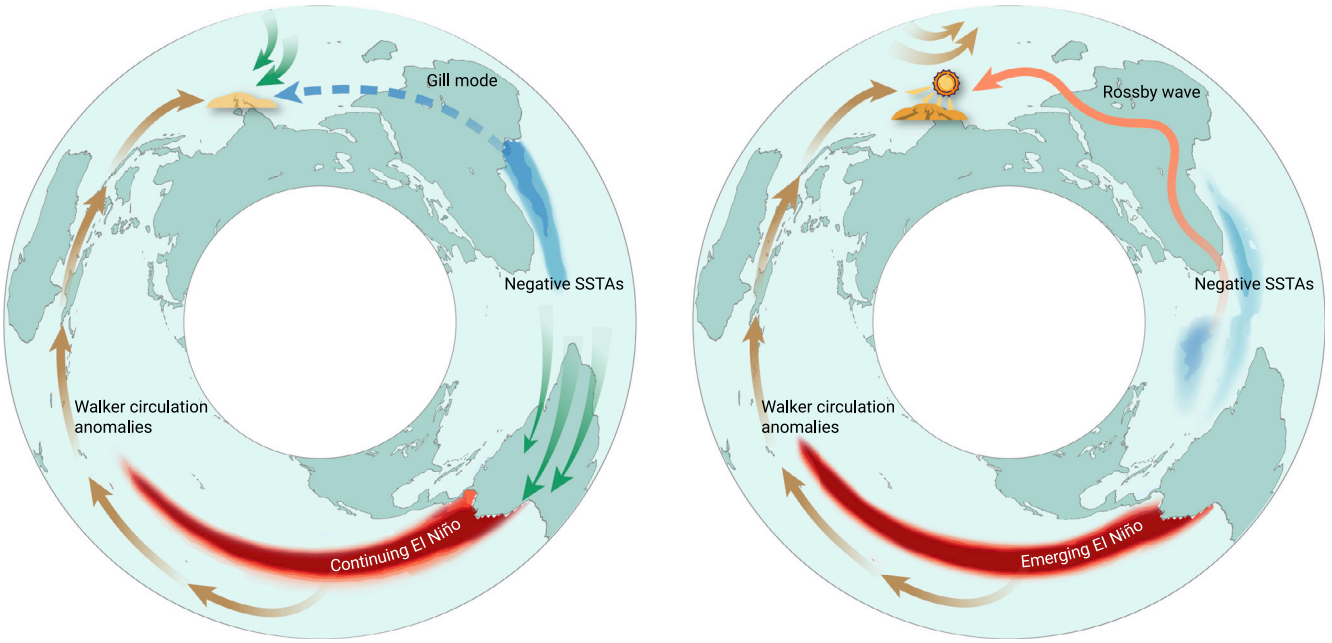

A 1979—1997 B 2000—2018

Public summary

- The relationship between ENSO and ISMR has been restoring since 1999/2000
- The transition of ENSO's evolution, continuing or emerging, is the dominant factor
- The response of tropical Atlantic SSTAs to ENSO's evolution are the crucial bridge

Article

Restored relationship between ENSO and Indian summer monsoon rainfall around 1999/2000

Xianke Yang[1,2] **and Ping Huang**[1,3,*]

[1]Center for Monsoon System Research, Institute of Atmospheric Physics, Chinese Academy of Sciences, Beijing 100190, China

[2]University of Chinese Academy of Sciences, Beijing 100049, China

[3]State Key Laboratory of Numerical Modeling for Atmospheric Sciences and Geophysical Fluid Dynamics, Institute of Atmospheric Physics, Chinese Academy of Sciences, Beijing 100190, China

*Correspondence: huangping@mail.iap.ac.cn

Received: November 15, 2020; Accepted: March 30, 2021; Published Online: April 2, 2021; https://doi.org/10.1016/j.xinn.2021.100102

Citation: Yang X. and Huang P. (2021). Restored relationship between ENSO and Indian summer monsoon rainfall around 1999/2000. The Innovation **2(2)**, 100102.

El Niño–Southern Oscillation (ENSO) was identified as the dominant predictor for the Indian summer monsoon rainfall (ISMR) in the early 1900s. An apparent weakening of the ENSO–ISMR relationship has been observed since the 1970s. Here, we found a clear restoration of the ENSO–ISMR relationship since 1999/2000. This restoring relationship is closely linked to the interdecadal transition of ENSO evolution and the associated sea surface temperature anomalies (SSTAs) over the tropical Atlantic. During 1979–1997, summer ENSO events mainly continued from the previous winter, which can drive apparent Atlantic Niña SSTAs to offset ENSO's impact on ISMR and weaken the ENSO–ISMR relationship. In contrast, when ENSO events newly emerge from late spring, as they have done more recently during 2000–2018, the associated tropical Atlantic SSTAs are weak and shift to the tropical North Atlantic, which can offset the contribution of Atlantic Niña and reinforce the ENSO–ISMR relationship. We identified that the diversity of ENSO's evolution, continuing from the previous winter or emerging from late spring, is the dominant factor perturbing the ENSO–ISMR relationship in recent epochs, with tropical Atlantic SSTAs as the crucial bridge. This finding should be considered in our efforts to improve ISMR prediction.

Keywords: ENSO–ISMR relationship; interdecadal transition; tropical Atlantic SSTAs; emerging ENSOs; continuing ENSOs

INTRODUCTION

Existing from June to September (JJAS), the Indian summer monsoon rainfall (ISMR) is a vital annual source of rainfall for the most densely populated areas of the Indian subcontinent, and can exert tremendous impacts on India's agricultural production and economic activities, as well as the livelihoods of the human population, which stands at more than one billion people.[1–3] The predictability of ISMR can be modulated by many factors, of which El Niño–Southern Oscillation (ENSO) has been identified as the most essential since the beginning of the 20th century.[4,5] ISMR is often suppressed by downward Walker circulation anomalies during warm ENSO events, inducing an inverse relationship between ENSO and ISMR.[6,7]

However, the ENSO–ISMR relationship shows apparent interdecadal variations, the most recent of which manifests as a weakening since the 1970s.[8] This weakened ENSO–ISMR relationship has been repeatedly confirmed, but the mechanism underpinning the instability of the ENSO–ISMR relationship remains puzzling. Several hypotheses have been proposed in this regard, including a reduced signal-to-noise ratio of ENSO related to surface temperatures over Eurasia,[8] the transition of ENSO spatial "flavors,"[2,9,10] the phase transition of Atlantic Multidecadal Oscillation,[11,12] and the stochastic perturbation process.[13] Some other studies have attributed the reason to enhanced disturbances of other interannual variabilities, such as the Indian Ocean dipole (IOD),[4,14,15] the West African summer monsoon rainfall,[16] Atlantic circulations,[17] and Atlantic SSTAs.[18–21]

RESULTS

Restoration of the ENSO–ISMR relationship

In this study, we found that the ENSO–ISMR relationship has been restoring since the end of the 20th century (Figures 1A, S1, and S2). Based on the 19- and 21-year sliding correlation from 1871 to 2019, the ENSO–ISMR relationship (see supplemental information for definitions) weakened from 1979, as reported before, but experienced a new interdecadal transition at around 1999/2000. The restoring relationship did not depend on the selection of sliding windows (Figure S1) or Niño index (Figure S2B), and was confirmed by multiple datasets of rainfall and sea surface temperature (SST) (Figures S2D and S2E). In addition, the two possible outliers of extreme ENSO events (see supplemental information for outlier identification), 1983 and 1997, do not influence this conclusion (Figure S2A).

Based on the correlation between ENSO and ISMR, we divided the recent decades into two epochs: 1979–1997 and 2000–2018 with weak and strong ENSO–ISMR correlation, respectively (Table S1). (Two other strong correlation periods, 1931–1949 and 1956–1974, were selected for comparison [see supplemental information].) During 1979–1997, negative ENSO–ISMR regression coefficient was only apparent in northern India (Figures 2A and S3K), whereas it was significant across a vast area of central India during three strong periods (Figures 2B and S3). Correspondingly, the ENSO-related 850-hPa wind anomalies in central India transformed from westerly in 1979–1997 to easterly in 2000–2018, reducing monsoon-related water vapor transport and reinforcing the negative ENSO–ISMR relationship. Moreover, the ENSO-related northwesterly anomalies intensified over northeastern India, reducing the transportation of water vapor to eastern India and suppressing rainfall.

Potential factors modifying the ENSO–ISMR relationship

Anomalous Walker circulation in the upper troposphere has been considered as a decisive bridge through which the tropical central-eastern Pacific SSTAs associated with ENSO influence ISMR remotely.[8,22] However, the ENSO-related 200-hPa velocity potential anomalies, an indicator of Walker circulation, did not show an interdecadal shift from 1979–1997 to 2000–2018 over the Indian subcontinent, the Indian Ocean, and the equatorial central-eastern Pacific (Figure S4), although ENSO's amplitude is believed to have been decreasing since 1999/2000.[23,24]

The almost unchanged Walker circulation anomalies in the upper troposphere and the apparent shift in 850-hPa wind anomalies imply that the SSTAs in other tropical oceans associated with ENSO might contribute to the interdecadal shift of the ENSO–ISMR relationship through lower-troposphere systems. For the Indian Ocean, the warm tropical Indian Ocean (TIO) or positive IOD favors positive ISMR.[25–28] However, the ENSO–TIO relationship has been increasing since the 2000s (Figure S2C), which would weaken rather than reinforce the ENSO–ISMR relationship. The relationship between ENSO and IOD[26] or between ENSO and the tropical western Pacific[29] do not show the interdecadal transition (not shown), which cannot also explain the ENSO–ISMR restoration. Meanwhile, there was an apparent

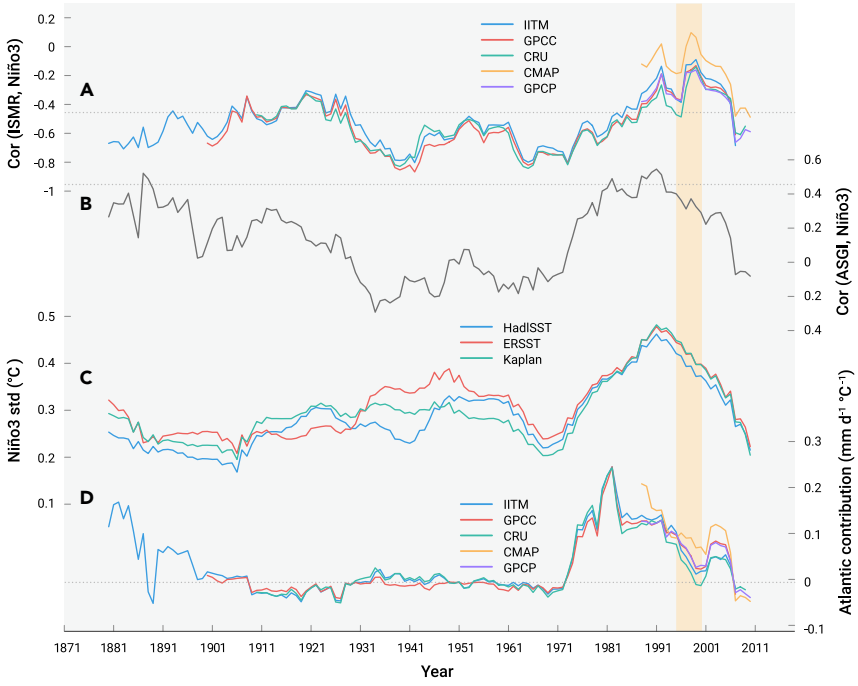

Figure 1. Correlation of Niño-3 index With ISMR and ASGI
(A) The 19-year sliding correlation coefficients between Niño-3 index and ISMR based on Indian data from the Institute of Tropical Meteorology (IITM), the Global Precipitation Climatology Centre (GPCC), the Climate Research Unit (CRU), CPC Merged Analysis of Precipitation (CMAP), and the Global Precipitation Climatology Project (GPCP).
(B) The 19-year sliding coefficient between Niño-3 index and ASGI. The dashed lines in (A) and (B) denote the 95% confidence level.
(C) The 19-year sliding standard deviation of the 4- to 7-year band-pass-filtered Niño-3 index.
(D) The role of Atlantic SSTAs in modifying the ENSO–ISMR relationship (units: mm d^{-1} $°C^{-1}$). The lightgrey shade indicates 1995–2000.

transition of the ENSO-related tropical SSTAs in the tropical Atlantic between 1979–1997 and 2000–2018 (Figures 2C and 2D), from a typical Atlantic Niña pattern to a pattern with weak SSTAs mainly located in the tropical North Atlantic. This result is insensitive to datasets as well (Figures S3E and S3F).

Therefore, the transition of ENSO-related SSTAs in the tropical Atlantic, rather than the Indian Ocean, may have resulted in the restoration of the ENSO–ISMR relationship. Actually, previous studies have demonstrated that the ENSO-related Atlantic Niña SSTAs might have been the reason behind the last weakening of the ENSO–ISMR relationship since the 1970s.[19,20,30,31] To validate the connection between the Atlantic SSTAs and the ENSO–ISMR relationship, an Atlantic SSTA gradient index (ASGI) was defined by the difference between the regionally averaged SSTAs in the tropical North Atlantic and in the tropical South Atlantic (two boxes in Figures 2C and 2D) to describe the SSTA pattern shift in the tropical Atlantic. The sliding correlation between the Niño-3 index and ASGI showed a persistent decrease since the mid-1990s, especially after 1999, which coincided well with the evolution of the ENSO–ISMR relationship (Figure 1B).

Role of the Atlantic SSTAs in ISMR

To illustrate the role played by the Atlantic SSTAs in ISMR, singular value decomposition (SVD) analysis was performed on the ISMR anomalies and Atlantic SSTAs from 1948 to 2018 with the ENSO-related signals removed or not (see Material and methods). As shown in Figures 3A and 3B, the heterogeneous correlation of the first SVD mode for ISMR, with ENSO-related signals removed, shows a pattern of wetness over central and northern India with westerly anomalies, and the tropical Atlantic SSTAs of the first SVD mode display a negative-south–positive-north dipole pattern. The spatial patterns do not depend on the selected period or datasets. The first SVD mode explains 60.11% of the total variance. The results of the SVD analysis, including ENSO-related signals (Figures 3C and 3D), are similar to those with ENSO signals removed, indicating that the ISMR–Atlantic SSTAs relationship is independent on ENSO. The homogeneous correlation maps (Figure S5) display similar spatial modes. Besides, the regression of ISMR onto ASGI is equivalent in 1979–1997 and 2000–2018 (Table S2), suggesting a stable relationship between ISMR and Atlantic SSTAs without apparent interdecadal transition in the recent epochs.

The SVD result suggests that the Atlantic Niña-like negative SSTAs can enhance ISMR but the negative tropical North Atlantic SSTAs can suppress ISMR. This tropical Atlantic–ISMR relationship is consistent with the conclusion in the previous studies and explained by the suggested mechanisms.[18–21,30,32–34] The positive tropical North Atlantic SSTAs can enhance ISMR through the large-scale monsoon circulation[32] and Rossby wave train.[33,35] Meanwhile, the negative Atlantic Niña SSTAs can increase ISMR through Asian jet,[31] Kelvin wave response,[21] and an abnormal westerly with a Gill–Matsuno-type quadrupole response.[18,19,30,34]

Under the tropical Atlantic–ISMR relationship, the Atlantic Niña SSTAs associated with ENSO during 1979–1997 (Figure 2C) were able to enhance ISMR and weaken the negative ENSO–ISMR relationship, whereas the negative tropical North Atlantic SSTAs during 2000–2018 (Figure 2D) would offset the impact of Atlantic Niña SSTAs, enhancing the ENSO–ISMR relationship. Accordingly, there is currently a persistent restoration of the ENSO–ISMR relationship, along with the pattern shift of ENSO-related Atlantic SSTAs.

But why did the ENSO-related tropical Atlantic SSTAs have such an interdecadal shift? A recent study[36] revealed that the ENSO–Atlantic Niño linkage is largely determined by the duration of ENSO events. The response of the tropical Atlantic is noticeable only during multi-year ENSO events in which the summer ENSO SSTAs continue from the previous winter, because the Atlantic SST needs a sufficiently long time to respond to ENSO SSTAs and is sensitive only in March–May.

Interdecadal transition of ENSO's typical periods and Atlantic response

In Figures 4A and S6A, the wavelet analysis for the seasonal Niño-3 index shows that the typical period of ENSO has an apparent interdecadal shift, consistent with recent findings.[23,24] ENSO was dominated by a 4- to 7-year period during 1978–1999, and then shifted to a 2- to 4-year period after 2000. This interdecadal variation of ENSO's period corresponds to the variation in ENSO's evolution. The time-averaged wavelet power spectra of the Niño-3 index (right panel in Figure 4A) has two peaks in the 3.4- and 5.3-year periods, respectively, which corresponds to different durations of ENSO events. The sliding standard deviation of the 4- to 7-year band-pass-filtered Niño-3 index (Figure 1C) also illustrates the interdecadal variation of ENSO's typical period, a 4- to 7-year period ENSO increasing from the 1970s and

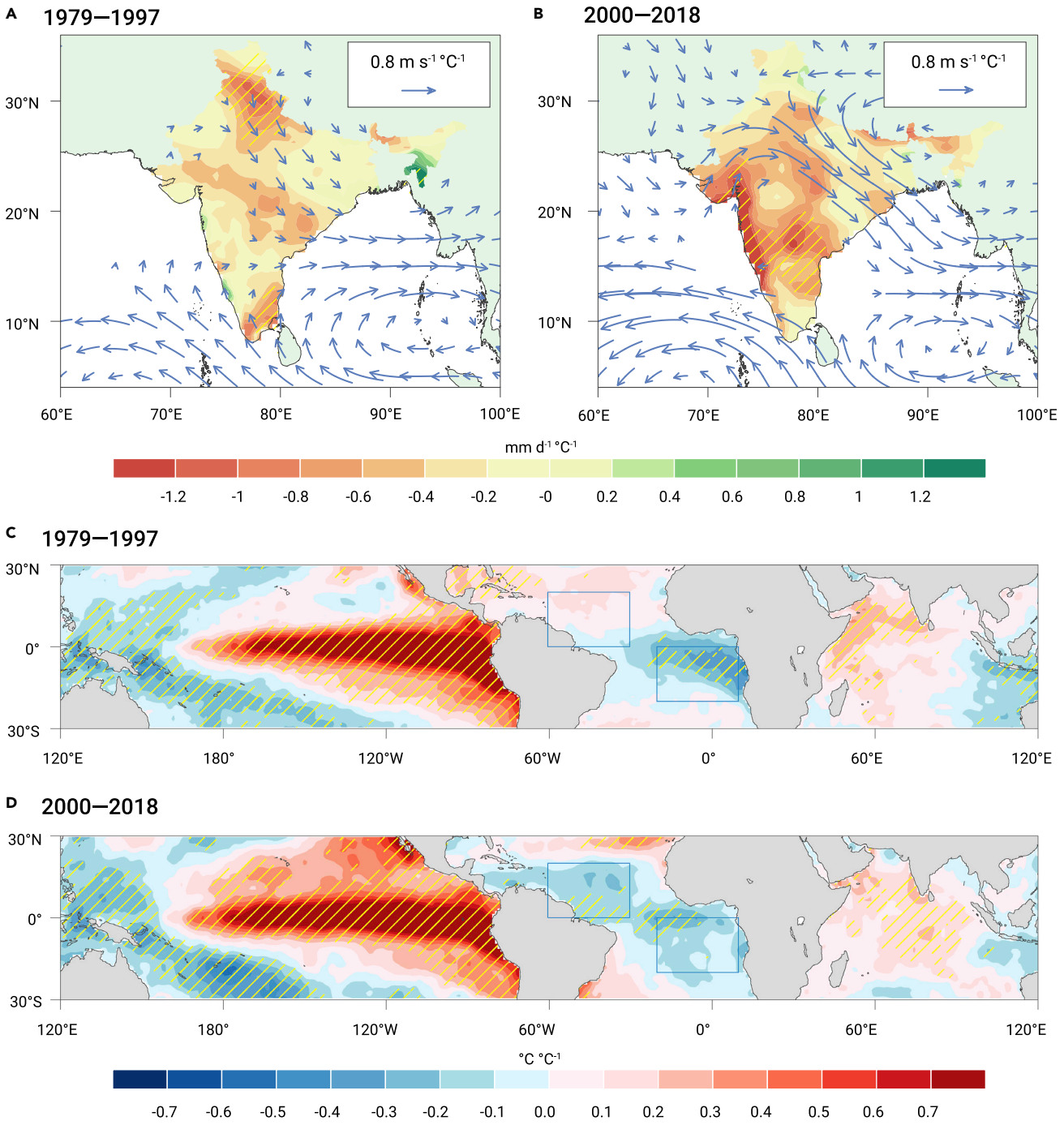

Figure 2. Regression of ISMR anomalies and tropical SSTAs onto Niño-3 index (A and B) The spatial pattern of the regression of ISMR from CRU onto Niño-3 index during (A) 1979–1997 and (B) 2000–2018. Vectors in (A) and (B) are the regression of 850-hPa wind anomalies onto the Niño-3 index. (C and D) The regression of tropical SSTAs onto Niño-3 index. In (C)–(D), the correlations exceeding 95% confidence level are hatched. Blue boxes denote the regions to define ASGI.

decreasing from the 1990s. As shown by the lead-lag correlation between the monthly equatorial SSTAs and summer Niño-3 index in 1979–1997 and 2000–2018 (Figures 4B and 4C), the equatorial Pacific summer SSTAs often continued from the previous winter during 1979–1997 (hereafter referred to as "continuing ENSOs"), whereas they often newly emerged from late spring in the more recent period of 2000–2018 (hereafter referred to as "emerging ENSOs").

The response of the equatorial Atlantic SSTAs was different during these two "flavors" of ENSO evolution (Figures 6A, 6B, S8A, and S8B). When the continuing ENSOs dominated during 1979–1997 (Figures 6D and S8C), the equatorial Atlantic SSTAs developed from April to June, responding to the simultaneous tropical Pacific SSTAs. In contrast, during 2000–2018 (Figures 6E and S8D), dominated by emerging ENSOs, the Atlantic SSTAs could not develop when the tropical Pacific SSTAs were weak in March–May, which is the sensitive season for tropical Atlantic SSTAs to develop.[36] The sliding ENSO–Atlantic correlation (Figure 1B) is significantly correlated to the sliding standard deviation of the 4- to 7-year band-pass-filtered Niño-3 index (Figure 1C) with a correlation coefficient 0.8 after the 1950s.

The impact of these two distinct evolutions of ENSO, i.e., continuing and emerging, on Atlantic SSTAs and the resultant modification of the

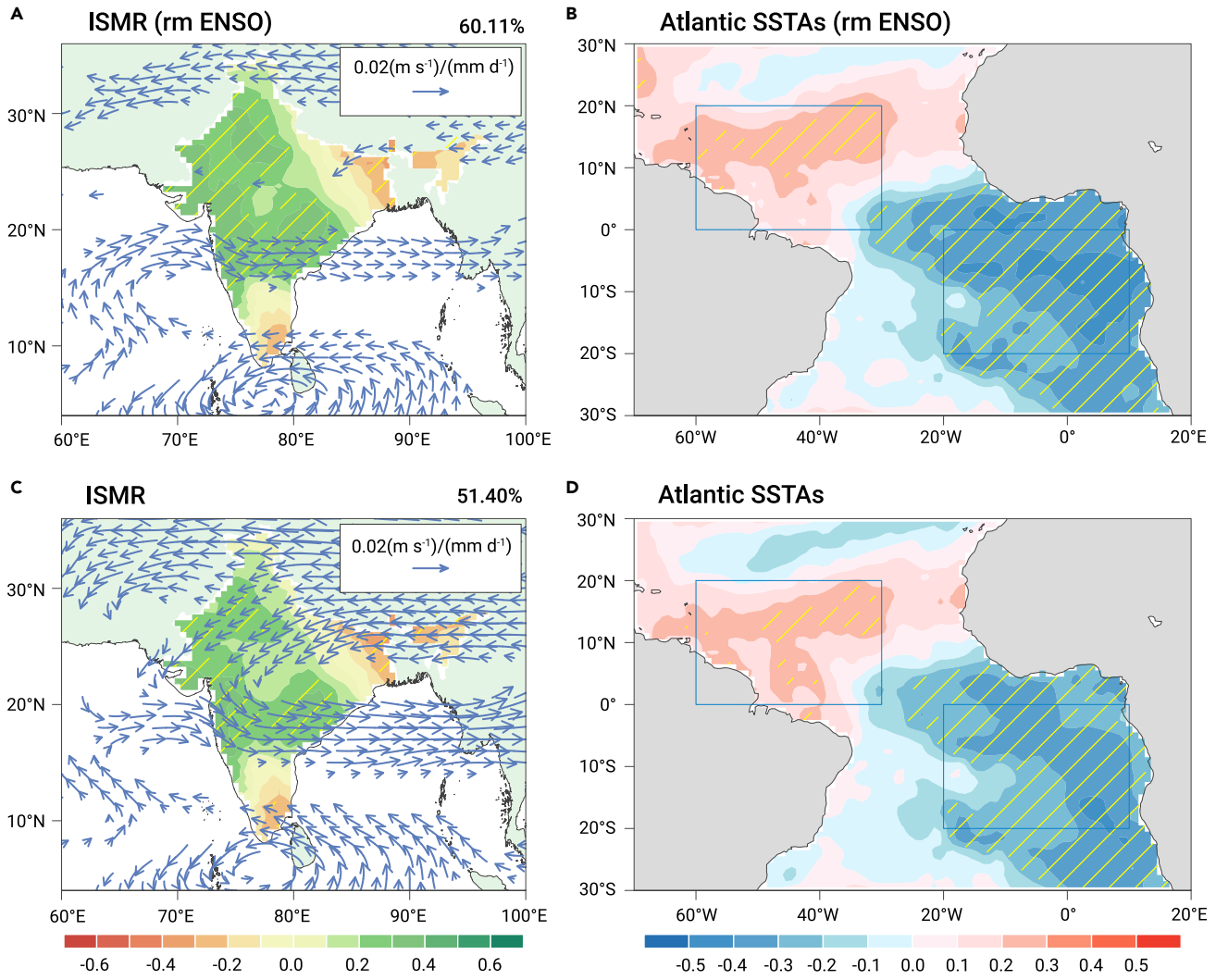

Figure 3. Heterogeneous correlation maps of the first mode of the SVD analysis for the tropical Atlantic SSTAs (HadISST) and ISMR anomalies (CRU) in 1948–2018 (A and B) The first SVD mode of (A) the ISMR pattern and (B) the tropical Atlantic SSTA pattern with ENSO-related signals removed. Vectors in (A) are the regression of 850-hPa wind anomalies onto the ISMR-related first principal component. (C and D) As in (A and B), but for the original tropical Atlantic SSTAs (HadISST) and ISMR anomalies (CRU) in which ENSO signals are not removed. The correlations exceeding 95% confidence level are hatched.

ENSO–ISMR relationship, were reexamined using composite analysis. Based on the evolution of the Niño-3 index (Figure 5) and the reliability of SST datasets, we defined continuing and emerging ENSO events from 1948 to 2018 (see Material and methods). The composited SSTAs for the two ENSO flavors describe the distinct SSTA evolutions well (Figures S7A and S7B). The proportion of continuing ENSOs from HadISST (Extended Reconstructed Sea Surface Temperature [ERSST]) decreases from 78% (60%) during 1979–1997 to 50% (29%) during 2000–2018. Consequently, the composite SSTA for ENSOs in 1979–1997 and 2000–2018 resembles that for continuing ENSOs and emerging ENSOs, respectively (Figures S7C and S7D). This result verifies the interdecadal shift of the ENSO flavor from one of continuing events to emerging events around 1999/2000.

The composite tropical Atlantic SSTAs associated with ENSO further support the conclusion from the linear correlation analysis (Figures 4B and 4C). During the continuing ENSOs and the ENSOs in 1979–1997, the equatorial southeastern Atlantic SSTAs developed from March–May and sustained to boreal summer, whereas there was no apparent Atlantic SSTA response to the ENSOs in boreal summer during the emerging ENSOs and ENSOs in 2000–2018 (Figure S7). Unsurprisingly, distinct Atlantic SSTAs could also be observed in the spatial pattern of tropical SSTAs in boreal summer (Figures 6 and S8).

Forced by the different Atlantic SSTA patterns, the composite ISMR anomalies are very distinct between the continuing and emerging ENSO events (Figures 7A, 7B, S8G, and S8H). The reverse ISMR anomalies are significant in the emerging ENSOs but very weak in the continuing ENSOs, and pronounced easterly anomalies over central India during the emerging ENSOs contribute to suppressing the ISMR. This result indicates that the flavor of ENSO's evolution, with distinct tropical Atlantic SSTAs, is the dominant factor determining the significance of the ENSO–ISMR relationship. Under the interdecadal transition of ENSO's evolution, the ENSO–ISMR relationship during 2000–2018 was significant because emerging ENSOs dominated, whereas the ENSO–ISMR was weak during 1979–1997 when continuing ENSOs dominated (Figures 7D, 7E, S8I, and S8J).

To quantify the role of Atlantic SSTAs in modifying the ENSO–ISMR relationship, an index (Figure 1D) is defined by the product of the sliding regression of ASGI onto the Niño-3 index and the sliding regression of ISMR onto ENSO-removed ASGI. The role of Atlantic SSTAs began to increase from the 1970s and decreased around the 1990s, corresponding to the two transition nodes of the ENSO–Atlantic relationship and the ENSO–ISMR relationship. This index is on the same order of magnitude as the regression of ISMR onto the Niño-3 index during 1979–1997 (Figure 2A; Table S2), suggesting that the transition of the Atlantic contribution plays a critical role in the recent two transition of the ENSO–ISMR relationship.

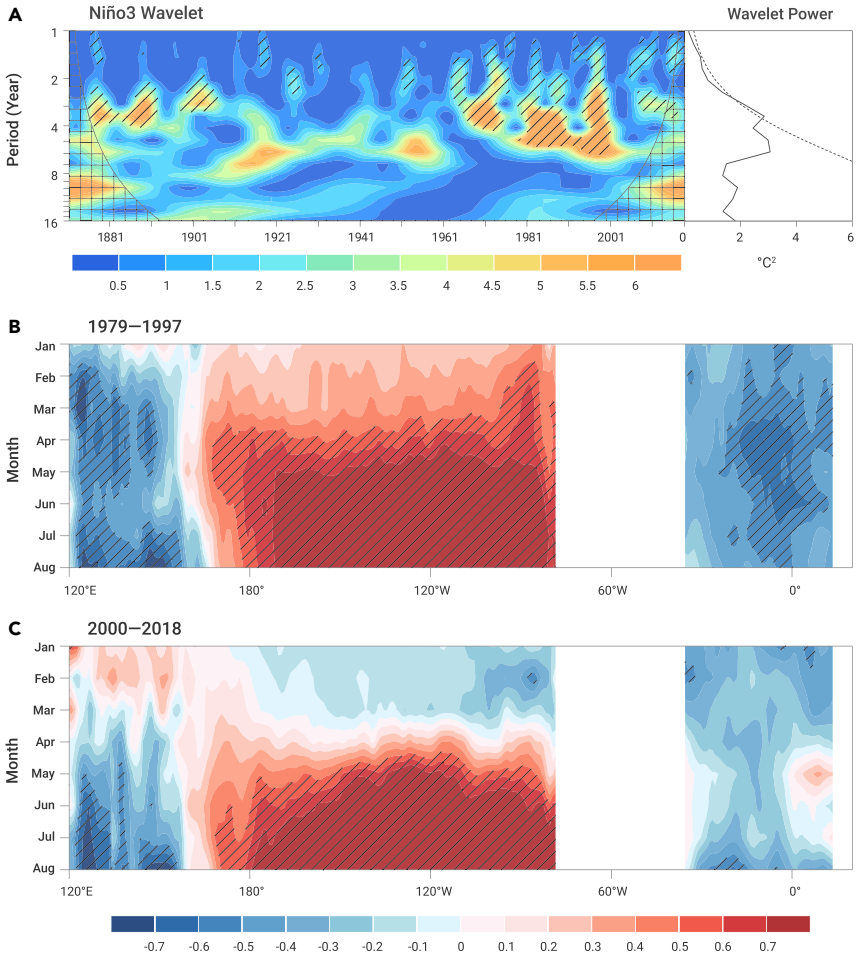

Figure 4. Wavelet analysis for seasonal Niño-3 index and the lead-lag correlation between summer Niño-3 index and equatorial SSTAs (A) The wavelet power spectrum and wavelet spectral coherence of the seasonal Niño-3 index from 1871 to 2018 using the Morlet wavelet. The results exceeding the 95% confidence level for the red-noise null hypothesis are hatched in the left column. Also shown are the time-averaged wavelet power spectrum (solid lines) and the threshold exceeding the 95% confidence level (dashed lines) in the right column.
(B) Lead-lag correlation between the JJAS Niño-3 index and monthly equatorial SSTAs, the 2.5°S–2.5°N mean for the Pacific (120°E–60°W), and the 5°S–10°S mean for the Atlantic (60°W–20°E) in 1979–1997.
(C) As in (B) but for 2000–2018. The results in (B and C) exceeding the 95% confidence level are hatched.

DISCUSSION

Apart from the Atlantic SSTAs, there are also different SSTAs in the tropical Pacific between ENSOs in 1979–1997 and 2000–2018 (Figures 6C and 6F). Firstly, we checked the tropical rainfall anomalies, which indicate anomalous convective heating directly induced by SSTAs, between continuing and emerging ENSO, as well as between ENSOs in 2000–2018 and in 1979–1997. There are no apparently different convective rainfall anomalies in the equational central-eastern Pacific (Figure S10). This result indicates that the slightly different ENSO SSTAs in the central-eastern Pacific are not the direct reason for the interdecadal transition.

Besides, since central Pacific (CP) ENSOs are more frequent than eastern Pacific (EP) ENSOs during 2000–2018,[2,23,24] we further distinguished all ENSO events into EP and CP types (see the supplemental information) to check the possible role of the spatial pattern transition of ENSOs. As expected, the spatial pattern transition of ENSO from 1979–1997 to 2000–2018 shows a typical transition from EP ENSOs to CP ENSOs (Figure S9). However, the ISMR anomalies during CP ENSOs are much weaker than those during EP ENSOs (Figures S9G and S9H), indicating that the ENSO–ISMR relationship should be weakened when CP ENSOs appeared more frequently (Figure S9K). This hypothesis conflicts with the observed restoration of the ENSO–ISMR relationship with more frequent CP ENSOs in 2000–2018 (Figures S9K and S9L). Moreover, the different Atlantic SSTAs between ENSOs in 2000–2018 and in 1979–1997 are distinct from those between CP and EP ENSOs, indicating that

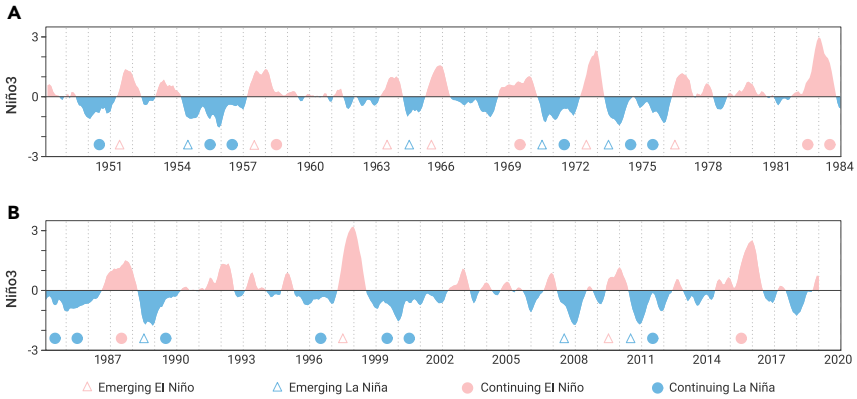

Figure 5. The 3-month running mean of the Niño-3 index and the defined continuing and emerging ENSOs Circles and triangles denote the continuing and emerging ENSOs (light red for El Niño and light blue for La Niña) during (A) 1948–1983 and (B) 1984–2018, respectively.

Article

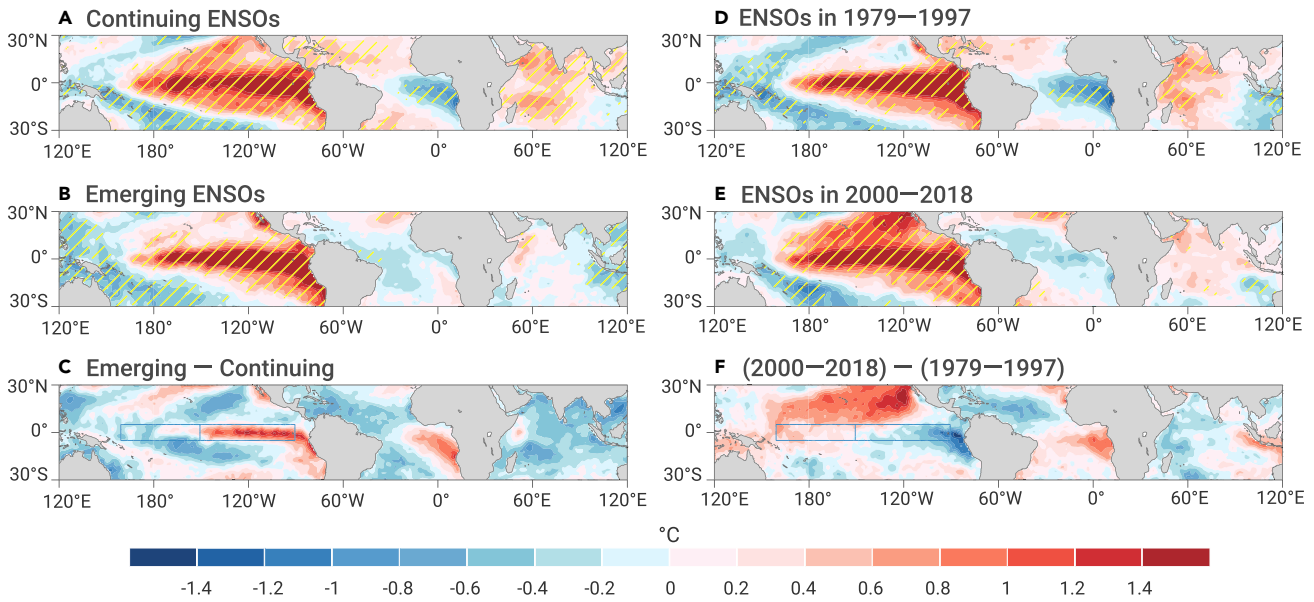

Figure 6. Composite tropical SSTAs in different ENSO groups Composite tropical SSTAs for (A) continuing ENSOs, (B) emerging ENSOs, and (D) ENSOs in 1979–1997, as well as (E) ENSOs in 2000–2018. The results exceeding the 95% confidence level are hatched. The results of (B) minus (A) and (E) minus (D) are shown in (C and F), respectively.

the interdecadal transition of the Atlantic response to ENSO is not induced by the EP–CP transition. In the meantime, we further classified the cases of continuing and emerging ENSOs into CP and EP groups, in which EP (CP) ENSOs are identified when the Niño-3 index is stronger (weaker) than the Niño-4 index from all continuing and emerging ENSOs. The composite results are similar to Figure S9. These results demonstrate that the EP–CP transition of ENSO does not contribute to the recent restoration of ENSO–ISMR relationship.

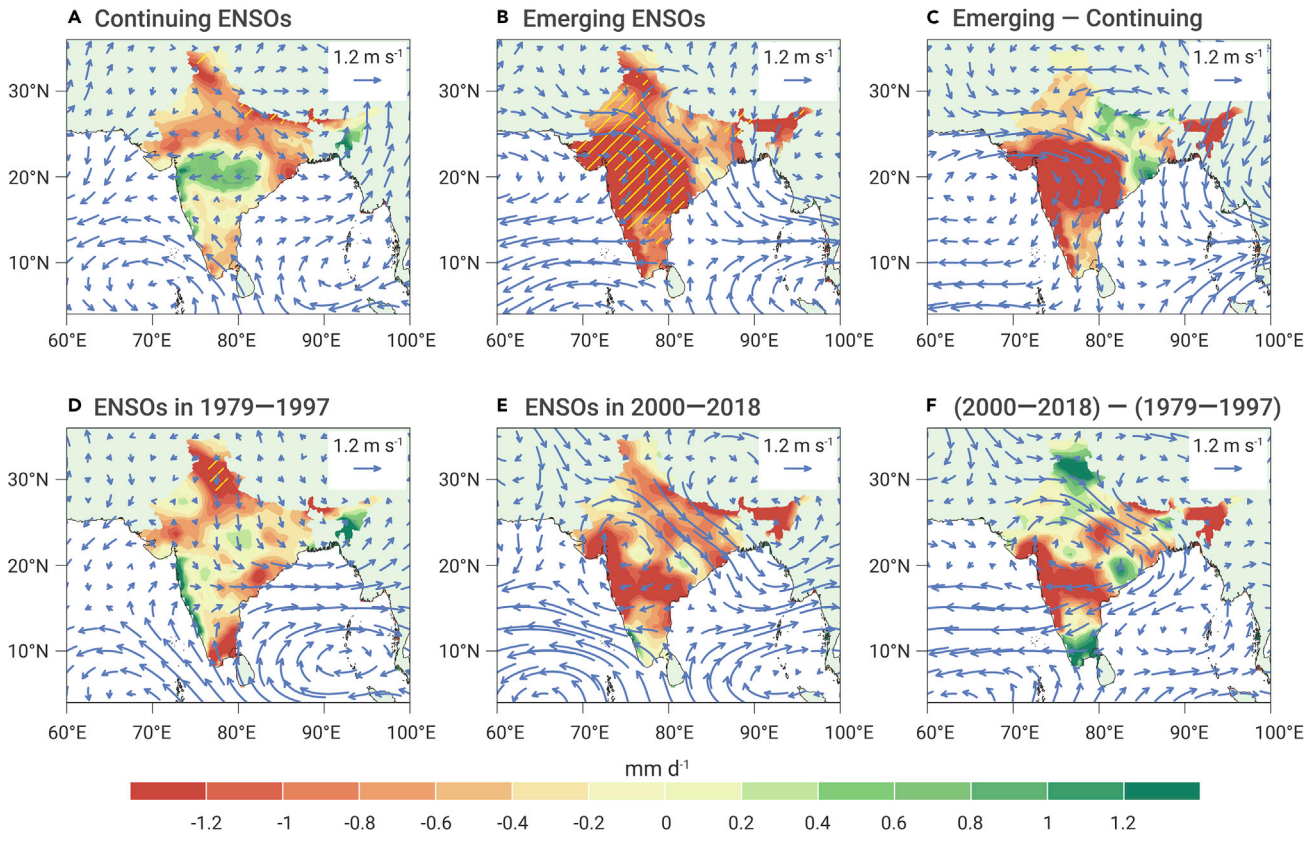

Figure 7. Composite ISMR anomalies and 850-hPa wind anomalies in different ENSO groups Composite for (A) continuing ENSOs, (B) emerging ENSOs, and (D) ENSOs in 1979–1997, as well as (E) ENSOs in 2000–2018. The results exceeding the 95% confidence level are hatched. The results of (B) minus (A) and (E) minus (D) are shown in (C and F), respectively.

Summary

By synthesizing multiple reanalysis datasets and *in-situ* observations, we have confirmed that the ENSO–ISMR relationship has been restoring since the end of the 20th century, despite ENSO's weakened amplitude in the meantime, and suggest that this restoration of the ENSO–ISMR relationship was induced by the interdecadal transition of ENSO's evolution and the associated tropical Atlantic SSTAs. As ENSO shifted from a 4- to 7-year period in 1978–1999 to a 2- to 4-year period after 2000,[23,24] the summer ENSO SSTAs mainly continued from the previous winter during 1979–1997, but were newly emerging from late spring in 2000–2018. During 1979–1997, with the greater number of continuing ENSOs, the tropical South Atlantic showed an apparently reverse SSTA, which was able to offset ENSO's impact on ISMR. In contrast, the ENSO-related Atlantic Niña SSTAs were weak and shifted to the tropical North Atlantic during the more frequent emerging ENSOs in 2000–2018, which has weakened the Atlantic perturbance and reinforced the negative ENSO–ISMR relationship.

This study highlights that the flavor of ENSO's evolution, i.e., continuing from the previous winter or emerging from late spring, is the dominant factor determining the significance of the ENSO–ISMR relationship via the effect of Atlantic SSTAs. There are two critical processes involved in this mechanism—the distinct response of Atlantic SSTAs to different ENSO evolutions, and the impact of Atlantic SSTAs on ISMR, which has also been quantified to characterize the contribution of the Atlantic SSTAs. Both these processes have been well verified by numerical experiments in previous studies.[18,19,34,36] The present study implies that the predictability of ISMR based on the summer ENSO signal could increase in the new era. Even so, we suggest the evolution of ENSO in preceding seasons and the simultaneous response of Atlantic SSTAs should be considered in ISMR prediction.

MATERIAL AND METHODS

Datasets used in the study

(1) All-Indian monthly rainfall from the Indian Institute of Tropical Meteorology for the period 1871–2016 (https://tropmet.res.in/static_pages.php?page_id=53). (2) The Global Precipitation Climatology Centre V2018 monthly precipitation product at a spatial resolution of 0.5° for the period 1901–2016.[37] (3) The Climate Research Unit TS v.4.03 monthly precipitation product at a spatial resolution of 0.5° for the period 1901–2018.[38] (4) The rest of the monthly precipitation data were from the Global Precipitation Climatology Project, v.2.3, and the CPC Merged Analysis of Precipitation, available at a spatial resolution of 2.5°, for the period 1979–2019.[39] (5) The National Climatic Data Center's ERSST, v.5, at a spatial resolution of 2.0° for the period 1854–2019.[40] (6) The Met Office Hadley Centre's sea surface temperature (HadISST) at a spatial resolution of 1.0° for the period 1870–2019.[41] (7) Monthly wind data with 17 levels were obtained from the National Centers for Environmental Prediction (NCEP) and National Center for Atmospheric Research reanalysis, available at a spatial resolution of 2.5° for the period 1948–2019.[42] (8) Monthly wind data with 28 levels were obtained from the NOAA-CIRES-DOE Twentieth Century Reanalysis (20CR), available at a spatial resolution of 1° for the period 1831–2015.[43]

The annual cycle, as well as the linear trend of all data, were removed to emphasize the interannual variability. The wind datasets are the combination of the NCEP from 1948 to 2019 and the 20CR from 1931 to 1947. The Niño-3 index was defined by the averaged SSTAs in JJAS over the region (90°W–150°W, 5°S–5°N) to represent ENSO in summer. The ISMR index was defined by the average rainfall in India. The ASGI was defined by the average difference in the SSTAs between the tropical North Atlantic (60°W–30°W, 0°–20°N) and the South Atlantic (20°W–10°E, 20°S–0°), denoted by the solid boxes in Figures 2C and 2D. The TIO index was defined by the averaged SSTAs in JJAS over the region (40°E–100°E, 20°S–20°N). The IOD index was defined by the average difference in the SSTAs between (50°E–70°E, 10°S–10°N) and (90°E–110°E, 10°S–0°).

Linear removal method

To isolate the component in the Atlantic SSTAs and ISMR anomalies independent of ENSO, residual time series were calculated based on linear regression following the method of An[44]:

$$\xi_{remove} = \xi - Z \times \frac{cov(\xi, Z)}{var(Z)}, \qquad \text{(Equation 1)}$$

where ξ and Z represent the time series of ISMR (or Atlantic SSTAs) and ENSO, respectively, *cov* indicates the covariance between two variables, and ***var*** indicates the variance of ENSO.

SVD

The SVD method was used to find the coupled patterns between the ISMR and Atlantic SSTAs.[45]

Continuing and emerging ENSOs

The continuing and emerging ENSOs were defined based on the evolution of the 3-month running mean of the Niño-3 index. First, we considered two situations for the continuing ENSOs—namely, the slowly decaying events and the developing events since the previous winter. For the slowly decaying situation, a continuing ENSO event was identified when the average Niño-3 index of Oct(−1)–Jan(0) was greater than 0.5 (below −0.5) standard deviation (STD), became greater than 0.5 (below −0.5) STD in any month during March(0)–May(0), and remained positive (negative) during the single months of JJAS(0). For the developing events since the previous winter, a continuing ENSO event was identified when the Niño-3 index was greater than 0.75 (below −0.75) STD in any month from October(−1) to May(0), accompanied by positive (negative) values for eight single months, and the JJAS(0)-mean Niño-3 index was greater than 0.5 (below −0.5) STD. Second, an emerging ENSO event was identified when the JJAS(0)-mean Niño-3 index was greater than 0.75 (below −0.75) STD but the year was not defined as a continuing ENSO event. Based on this definition, we identified 19 continuing ENSOs (6 El Niños and 13 La Niñas, marked by circles in Figure 5) and 15 emerging ENSOs (8 El Niños and 7 La Niñas, marked by triangles in Figure 5) using HadISST from 1948 to 2018. All composite results were based on El Niño minus La Niña.

REFERENCES

1. Jin, Q., and Wang, C. (2017). A revival of Indian summer monsoon rainfall since 2002. Nat. Clim. Change ***7***, 587–594.
2. Wang, B., Xiang, B., Li, J., et al. (2015). Rethinking Indian monsoon rainfall prediction in the context of recent global warming. Nat. Commun. ***6***, 7154.
3. Mishra, V., Smoliak, B.V., Lettenmaier, D.P., et al. (2012). A prominent pattern of year-to-year variability in Indian summer monsoon rainfall. P. Natl. Acad. Sci. USA. ***109***, 7213–7217.
4. Ashok, K., Guan, Z., and Yamagata, T. (2001). Impact of the Indian Ocean dipole on the relationship between the Indian monsoon rainfall and ENSO. Geophys. Res. Lett. ***28***, 4499–4502.
5. Walker, G.T. (1933). Seasonal weather and its prediction. Nature ***132***, 805–808.
6. Webster, P.J., and Palmer, T.N. (1997). The past and the future of El Niño. Nature ***390***, 562–564.
7. Pant, G.B., and Parthasarathy, S.B. (1981). Some aspects of an association between the Southern Oscillation and Indian summer monsoon. Arch. Meteorol. Geophy. B. ***29***, 245–252.
8. Kumar, K.K., Rajagopalan, B., and Cane, M.A. (1999). On the weakening relationship between the Indian monsoon and ENSO. Science ***284***, 2156–2159.
9. Kumar, K.K., Rajagopalan, B., Hoerling, M., et al. (2006). Unraveling the mystery of Indian monsoon failure during El Niño. Science ***314***, 115–119.
10. Fan, F., Dong, X., Fang, X., et al. (2017). Revisiting the relationship between the South Asian summer monsoon drought and El Niño warming pattern. Atmos. Sci. Lett. ***18***, 175–182.
11. Chen, W., Dong, B., and Lu, R. (2010). Impact of the Atlantic ocean on the multidecadal fluctuation of El Niño–Southern Oscillation–south Asian monsoon relationship in a coupled general circulation model. J. Geophys. Res.-Atmos. ***115***, D17109.
12. Lu, R., Chen, W., and Dong, B. (2008). How does a weakened Atlantic thermohaline circulation lead to an intensification of the ENSO-South Asian summer monsoon interaction? Geophys. Res. Lett. ***35***, L08706.
13. Yun, K.-S., and Timmermann, A. (2018). Decadal monsoon-ENSO relationships reexamined. Geophys. Res. Lett. ***45***, 2014–2021.
14. Krishnaswamy, J., Vaidyanathan, S., Rajagopalan, B., et al. (2014). Non-stationary and non-linear influence of ENSO and Indian Ocean dipole on the variability of Indian monsoon rainfall and extreme rain events. Clim. Dynam. ***45***, 175–184.
15. Chowdary, J.S., Xie, S.-P., Tokinaga, H., et al. (2012). Interdecadal variations in ENSO teleconnection to the Indo–western Pacific for 1870–2007. J. Clim. ***25***, 1722–1744.
16. Srivastava, G., Chakraborty, A., and Nanjundiah, R.S. (2019). Multidecadal see-saw of the impact of ENSO on Indian and West African summer monsoon rainfall. Clim. Dynam. ***52***, 6633–6649.
17. Chang, C.-P., Harr, P., and Ju, J. (2000). Possible roles of Atlantic circulations on the weakening Indian monsoon rainfall–ENSO relationship. J. Clim. ***14***, 2376–2380.
18. Kucharski, F., Bracco, A., Yoo, J.H., et al. (2009). A Gill–Matsuno-type mechanism explains the tropical Atlantic influence on African and Indian monsoon rainfall. Q. J. Roy. Meteorol. Soc. ***135***, 569–579.
19. Kucharski, F., Bracco, A., Yoo, J.H., et al. (2007). Low-frequency variability of the Indian monsoon–ENSO relationship and the tropical Atlantic: the "weakening" of the 1980s and 1990s. J. Clim. ***20***, 4255–4266.
20. Yadav, R.K. (2016). On the relationship between east equatorial Atlantic SST and ISM through Eurasian wave. Clim. Dynam. ***48***, 281–295.

21. Sabeerali, C.T., Ajayamohan, R.S., Bangalath, H.K., et al. (2019). Atlantic zonal mode: an emerging source of Indian summer monsoon variability in a warming world. Geophys. Res. Lett. ***46***, 4460–4467.
22. Seetha, C.J., Varikoden, H., Babu, C.A., et al. (2019). Significant changes in the ENSO-monsoon relationship and associated circulation features on multidecadal timescale. Clim. Dynam. ***54***, 1491–1506.
23. Hu, Z.Z., Kumar, A., Huang, B.H., et al. (2020). The interdecadal shift of ENSO properties in 1999/2000: a review. J. Clim. ***33***, 4441–4462.
24. He, Z., Wang, W., Wu, R., et al. (2020). Change in coherence of summer rainfall variability over the Western Pacific around the early 2000s: ENSO influence. J. Clim. ***33***, 1105–1119.
25. Vibhute, A., Halder, S., Singh, P., et al. (2020). Decadal variability of tropical Indian Ocean sea surface temperature and its impact on the Indian summer monsoon. Theor. Appl. Climatol. ***141***, 551–566.
26. Hrudya, P.H., Varikoden, H., and Vishnu, R. (2021). A review on the Indian summer monsoon rainfall, variability and its association with ENSO and IOD. Meteorol. Atmos. Phys. ***133***, 1–14.
27. Chowdary, J.S., Harsha, H.S., Gnanaseelan, C., et al. (2017). Indian summer monsoon rainfall variability in response to differences in the decay phase of El Niño. Clim. Dynam. ***48***, 2707–2727.
28. Wang, Z., Li, G., and Yang, S. (2018). Origin of Indian summer monsoon rainfall biases in CMIP5 multimodel ensemble. Clim. Dynam. ***51***, 755–768.
29. Li, G., Xie, S.P., He, C., et al. (2017). Western Pacific emergent constraint lowers projected increase in Indian summer monsoon rainfall. Nat. Clim. Change ***7***, 708–712.
30. Kucharski, F., Bracco, A., Yoo, J.H., et al. (2008). Atlantic forced component of the Indian monsoon interannual variability. Geophys. Res. Lett. ***35***, L04706.
31. Yadav, R.K., Srinivas, G., and Chowdary, J.S. (2018). Atlantic Niño modulation of the Indian summer monsoon through Asian jet. Npj Clim. Atmos. Sci. ***1***, 23.
32. Rong, X., Zhang, R., and Li, T. (2010). Impacts of Atlantic sea surface temperature anomalies on Indo-East Asian summer monsoon-ENSO relationship. Chin. Sci. Bull. ***55***, 2458–2468.
33. Yadav, R.K. (2009). Changes in the large-scale features associated with the Indian summer monsoon in the recent decades. Int. J. Climatol. ***29***, 117–133.
34. Kucharski, F., and Joshi, M.K. (2017). Influence of tropical South Atlantic sea-surface temperatures on the Indian summer monsoon in CMIP5 models. Q. J. Roy. Meteorol. Soc. ***143***, 1351–1363.
35. Rajeevan, M., and Sridhar, L. (2008). Inter-annual relationship between Atlantic sea surface temperature anomalies and Indian summer monsoon. Geophys. Res. Lett. ***35***, L21704.
36. Tokinaga, H., Richter, I., and Kosaka, Y. (2019). ENSO influence on the Atlantic Niño, revisited: multi-year versus single-year ENSO events. J. Clim. ***32***, 4585–4600.
37. Schneider, U., Finger, P., Meyer-Christoffer, A., et al. (2017). Evaluating the hydrological cycle over land using the newly-corrected precipitation climatology from the global precipitation climatology centre (GPCC). Atmosphere ***8***, 52.
38. Harris, I., Jones, P.D., Osborn, T.J., et al. (2014). Updated high-resolution grids of monthly climatic observations—the CRU TS3.10 dataset. Int. J. Climatol. ***34***, 623–642.
39. Adler, R.F., Huffman, G.J., Chang, A., et al. (2003). The version-2 Global Precipitation Climatology Project (GPCP) monthly precipitation analysis (1979–present). J. Hydrometeorol. ***4***, 1147–1167.
40. Huang, B., Thorne, P.W., Banzon, V.F., et al. (2017). Extended reconstructed sea surface temperature, version 5 (ERSSTv5): upgrades, validations, and intercomparisons. J. Clim. ***30***, 8179–8205.
41. Rayner, N.A., Parker, D.E., Horton, E.B., et al. (2003). Global analyses of sea surface temperature, sea ice, and night marine air temperature since the late nineteenth century. J. Geophys. Res.-Atmos. ***108***, 4407.
42. Kalnay, E., Kanamitsu, M., Kistler, R., et al. (1996). The NCEP/NCAR 40-year reanalysis project. B. Am. Meteorol. Soc. ***77***, 437–471.
43. Slivinski, L.C., Compo, G.P., Whitaker, J.S., et al. (2019). Towards a more reliable historical reanalysis: improvements for version 3 of the twentieth century reanalysis system. Q. J. Roy. Meteorol. Soc. ***145***, 2876–2908.
44. An, S.I. (2003). Conditional maximum covariance analysis and its application to the tropical Indian Ocean SST and surface wind stress anomalies. J. Clim. ***16***, 2932–2938.
45. Bretherton, C.S., Smith, C., and Wallace, J.M. (1992). An intercomparison of methods for finding coupled patterns in climate data. J. Clim. ***5***, 541–560.

ACKNOWLEDGMENTS

This work was supported by the National Key R&D Program of China (grant 2019YFA0606703), the National Natural Science Foundation of China (grants 41722504 and 41975116), and the Youth Innovation Promotion Association of the Chinese Academy of Sciences. Data and codes will be made available upon request to X.Y.

AUTHOR CONTRIBUTIONS

P.H. conceived the study. X.Y. and P.H. designed the analyses. X.Y. performed the analyses and made the figures. P.H. and X.Y. wrote the paper.

DECLARATION OF INTERESTS

The authors declare no competing interests.

SUPPLEMENTAL INFORMATION

Supplemental information can be found online at https://doi.org/10.1016/j.xinn.2021.100102.